Nanomechanical absorption spectroscopy of 2D materials with femtowatt sensitivity

To cite this article: Jan N Kirchhof *et al* 2023 *2D Mater.* **10** 035012

View the article online for updates and enhancements.

You may also like

2D Materials

PAPER

Nanomechanical absorption spectroscopy of 2D materials with femtowatt sensitivity

Jan N Kirchhof[1,*] [ID], Yuefeng Yu[1], Denis Yagodkin[1] [ID], Nele Stetzuhn[1,2], Daniel B de Araújo[1] [ID], Kostas Kanellopulos[3], Samuel Manas-Valero[4,5], Eugenio Coronado[4] [ID], Herre van der Zant[5] [ID], Stephanie Reich[1] [ID], Silvan Schmid[3] [ID] and Kirill I Bolotin[1,*] [ID]

1 Department of Physics, Freie Universität Berlin, Arnimallee 14, 14195 Berlin, Germany
2 Max-Born-Institut für Nichtlineare Optik und Kurzzeitspektroskopie, Max-Born-Straße 2A, 12489 Berlin, Germany
3 Institute of Sensor and Actuator Systems, TU Wien, Gusshausstrasse 27-29, 1040 Vienna, Austria
4 Instituto de Ciencia Molecular, Universidad de Valencia, Calle Catedrático José Beltrán 2, 46980 Paterna, Spain
5 Kavli Institute of Nanoscience, Delft University of Technology, Lorentzweg 1, Delft 2628 CJ, The Netherlands
* Authors to whom any correspondence should be addressed.

E-mail: jan.kirchhof@fu-berlin.de and kirill.bolotin@fu-berlin.de

Keywords: NEMS, resonator, silicon nitride, nanomechanical resonators, 2D materials, spectroscopy,
transition metal dichalcogenides (TMDs)

Supplementary material for this article is available online

Abstract

Nanomechanical spectroscopy (NMS) is a recently developed approach to determine optical
absorption spectra of nanoscale materials via mechanical measurements. It is based on measuring
changes in the resonance frequency of a membrane resonator vs. the photon energy of incoming
light. This method is a direct measurement of absorption, which has practical advantages
compared to common optical spectroscopy approaches. In the case of two-dimensional (2D)
materials, NMS overcomes limitations inherent to conventional optical methods, such as the
complications associated with measurements at high magnetic fields and low temperatures. In this
work, we develop a protocol for NMS of 2D materials that yields two orders of magnitude
improved sensitivity compared to previous approaches, while being simpler to use. To this end, we
use mechanical sample actuation, which simplifies the experiment and provides a reliable
calibration for greater accuracy. Additionally, the use of low-stress silicon nitride membranes as
our substrate reduces the noise-equivalent power to NEP $= 890$ fW $\sqrt{\mathrm{Hz}}^{-1}$, comparable to
commercial semiconductor photodetectors. We use our approach to spectroscopically characterize
a 2D transition metal dichalcogenide (WS_2), a layered magnetic semiconductor ($CrPS_4$), and a
plasmonic super-crystal consisting of gold nanoparticles.

1. Introduction

Nanomechanical resonators emerged as sensitive probes for minuscule forces [1–3] and atomic-scale masses [4–8]. By incorporating two-dimensional (2D) materials into nanomechanical resonators, the miniaturization of these devices has been pushed to the ultimate limit of atomic thickness. Along with this comes a massively reduced effective mass, increased resonance frequencies, easily accessible non-linearity, and the ability to tune resonance frequencies [9]. This technological boost allows using such resonators as sensors for light [10], magnetic fields [11, 12], sound

[6, 13–15], gases [6, 16] or even to study live bacteria [17].

Recently, the use of 2D materials-based resonators as fast and broadband optical spectrometers has been demonstrated [18]. In this nanomechanical spectroscopy approach (NMS), changes in the mechanical resonance frequency of a freely suspended 2D material are measured as a function of the illumination photon energy E_γ. From this, both real and imaginary components of the dielectric function can be extracted. In this measurement the material effectively acts as its own photodetector, leading to broadband sensitivity (UV-THz) of the approach. Furthermore,

unlike classical optical approaches, NMS can distinguish between scattered and absorbed light. Finally, NMS is suitable for nanostructures with dimensions smaller than a micron and is applicable at low temperatures and high magnetic fields. Whilst NMS has many fundamental advantages, it currently lacks the sensitivity provided by state-of-the-art optical approaches.

Here, we reduce the noise equivalent power of NMS by two orders of magnitude, down to NEP = 890 fW $\sqrt{\text{Hz}}^{-1}$. At the same time, we simplify the method by using mechanical actuation, which allows us to study electrically insulating materials, makes sample loading straightforward and provides a simple, but robust calibration. We use this improved method to spectroscopically characterize a range of 2D structures with high resolution. This includes WS$_2$, a classic binary transition metal dichalcogenide (TMD), CrPS$_4$, a layered magnetic semiconductor (ternary TMD), and a plasmonic meta-structure consisting of gold nanoparticles forming a super-crystal [19, 20].
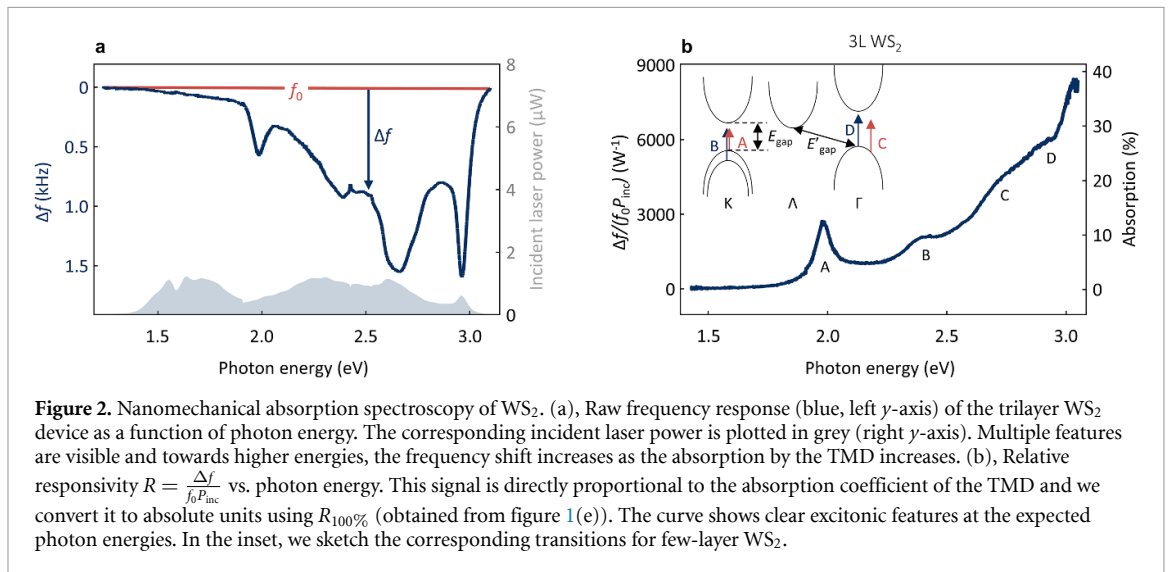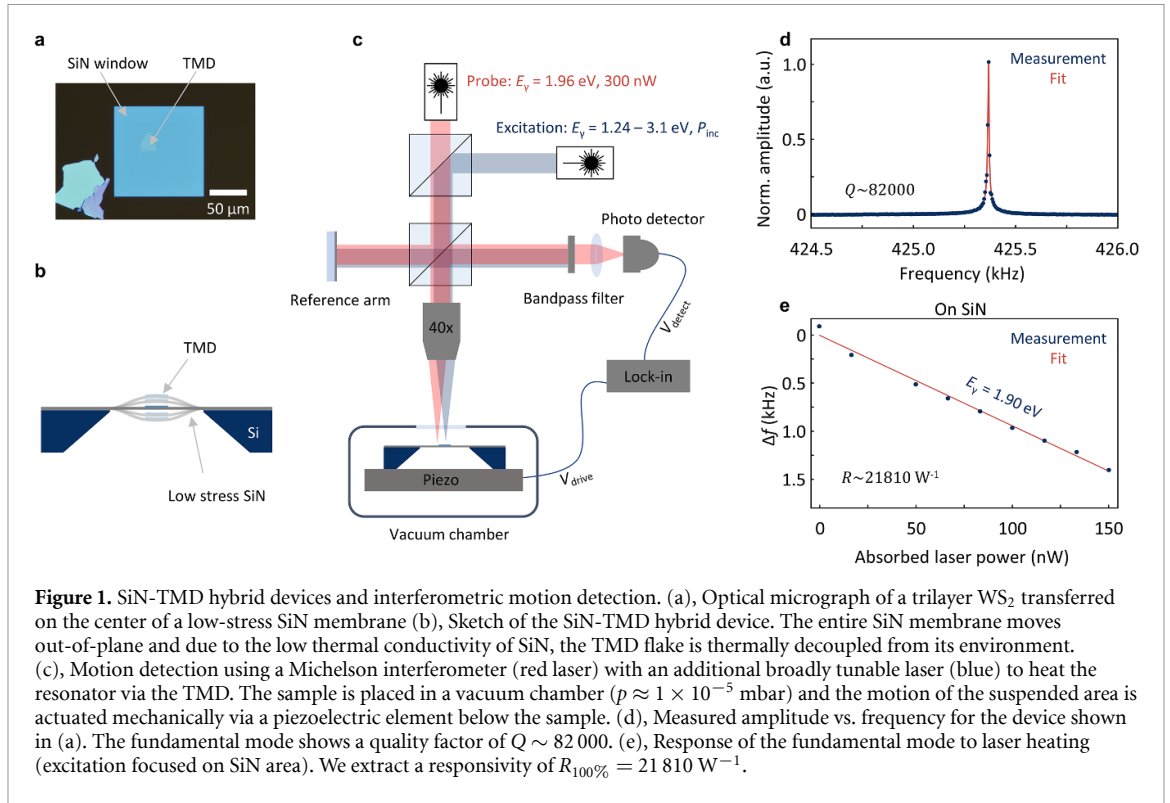
2. Results

2.1. Sample design

At the core of our device is a nanostructure or 2D material of interest that we place on top of a silicon nitride (SiN) membrane, thereby forming a hybrid resonator [18, 21, 22]. We use SiN for its excellent mechanical properties and record high quality factors (Q) [23–27]. The device is illuminated by a light source of tunable photon energy ($E_\gamma = 1.2$–3.1 eV). The absorption of light by the 2D material heats up the entire hybrid device. Due to thermal expansion, the in-plane tensile stress within the membrane is released and the resonance frequency downshifts. This downshift in frequency is proportional to the amount of absorbed laser power ($P_{\text{abs}}(E_\gamma)$) and allows us to perform absorption spectroscopy. To understand the measurement's underlying mechanics and optimize our sample design, we start by looking at the fundamental resonance of a square prestressed SiN membrane. The resonance frequency is given by $f_0 = \frac{1}{L}\sqrt{\frac{\sigma_0}{2\rho}}$, where L is the length, σ_0 the in-plane tensile stress and ρ the density. When the incoming light heats the material, the stress is reduced by $\Delta\sigma = \alpha\Delta T\frac{E}{1-\nu}$, where α is the thermal expansion coefficient, ΔT is the average temperature increase, E is the Young's modulus and ν is the Poisson's ratio. Here, ΔT is directly proportional to P_{abs}. The resulting frequency shift $\Delta f = f_0 - f$ can be approximated as $\Delta f \approx f_0\frac{\Delta\sigma}{2\sigma_0}$ [10, 23]. Thus, in order to maximize the frequency response to laser heating (responsivity) and ultimately improve the sensitivity of NMS, we aim to minimize the in-plane tensile stress σ_0 within

our membranes [23]. To do so, we choose SiN membranes ($L = 120$ μm, thickness $h = 50$ nm) grown by low-pressure chemical vapor deposition. By using a silicon-rich stoichiometry, we obtain membranes with low built-in stress. Thin layers of amorphous SiN also have a reduced thermal conductivity of $\kappa \approx 3$ W m^{-1} K^{-1} [28], which is beneficial for our experiments as it increases the temperature rise within our device in response to laser heating [29]. To complete the hybrid resonators, we transfer a 2D material of interest onto the SiN-membrane using the polydimethylsiloxane (PDMS) dry transfer technique [30]. Here, we ensure that we place the 2D material in the center of the membrane such that there are no thermal links to the rest of the substrate. An optical micrograph of a sample with a trilayer WS$_2$ is shown in figure 1(a) and schematically in a side view in figure 1(b).

The membrane's motion is actuated mechanically by a piezoelectric element below the sample and detected interferometrically using a HeNe laser ($E_\gamma = 1.96$ eV) with a probe power of 300 nW (red in figure 1(c)). A second wavelength-tunable excitation laser (blue in figure 1 (c)), allows us to controllably heat the resonator, whilst we monitor the changes in resonance frequency. Upon sweeping the actuation frequency we find a pronounced fundamental mode at $f_0 = 425.367$ kHz as shown in figure 1(d). From fitting a driven harmonic oscillator response to the experimental data, we estimate (the exact determination requires ring-down measurements) a quality factor of $Q = 82\,000$, comparable to previous results on similar samples [23]. Knowing f_0, L and $\rho = 3000$ m^3 kg^{-1} [23, 25], we calculate the stress in our membrane to be $\sigma_0 \approx 15.6$ MPa—much lower than commercially available SiN membranes (250–1000 MPa). All measurements are carried out at room temperature (stabilized) and at a pressure of $p \approx 1 \times 10^{-5}$ mbar. Next, we determine the responsivity of the resonator to absorbed light $R_{100\%} = \frac{\Delta f}{f_0 P_{\text{abs}}}$. To this end, we focus the probe and excitation beam (set to $E_\gamma = 1.9$ eV) on the SiN area close to the center of the sample and vary the laser power of the excitation laser from 0 to 30 μW. We use the known absorption ($Abs = 0.5\%$) of SiN at that photon energy [23] to convert the incident laser power to absorbed laser power ($P_{\text{abs}} = P_{\text{inc}}Abs$) and plot Δf vs. P_{abs} in figure 1(e). From a linear fit (red), we extract a responsivity of $R_{100\%} = 21\,810$ W^{-1}. We will use this quantity for the calibration of our measurements and to calculate the sensitivity of NMS. The measured $R_{100\%}$ is much higher than in previous approaches ($R_{100\%} = 180$ W^{-1}) [18]. At the same time, the Q of the improved system is more than an order of magnitude higher than in previous measurements (82 000 vs. 5000). Overall, we now have our material of interest implemented into a high quality

Figure 1. SiN-TMD hybrid devices and interferometric motion detection. (a), Optical micrograph of a trilayer WS$_2$ transferred on the center of a low-stress SiN membrane (b), Sketch of the SiN-TMD hybrid device. The entire SiN membrane moves out-of-plane and due to the low thermal conductivity of SiN, the TMD flake is thermally decoupled from its environment. (c), Motion detection using a Michelson interferometer (red laser) with an additional broadly tunable laser (blue) to heat the resonator via the TMD. The sample is placed in a vacuum chamber ($p \approx 1 \times 10^{-5}$ mbar) and the motion of the suspended area is actuated mechanically via a piezoelectric element below the sample. (d), Measured amplitude vs. frequency for the device shown in (a). The fundamental mode shows a quality factor of $Q \sim 82\,000$. (e), Response of the fundamental mode to laser heating (excitation focused on SiN area). We extract a responsivity of $R_{100\%} = 21\,810$ W^{-1}.

Figure 2. Nanomechanical absorption spectroscopy of WS$_2$. (a), Raw frequency response (blue, left y-axis) of the trilayer WS$_2$ device as a function of photon energy. The corresponding incident laser power is plotted in grey (right y-axis). Multiple features are visible and towards higher energies, the frequency shift increases as the absorption by the TMD increases. (b), Relative responsivity $R = \frac{\Delta f}{f_0 P_{\text{inc}}}$ vs. photon energy. This signal is directly proportional to the absorption coefficient of the TMD and we convert it to absolute units using $R_{100\%}$ (obtained from figure 1(e)). The curve shows clear excitonic features at the expected photon energies. In the inset, we sketch the corresponding transitions for few-layer WS$_2$.

mechanical hybrid resonator, that is engineered to strongly react to absorbed light.

2.2. Nanomechanical absorption measurements
After optimizing our mechanical system as a sensor for detecting light, we use it to perform absorption spectroscopy on several candidates, starting with the 2D semiconductor WS$_2$ (trilayer). To do so, we track the frequency of the fundamental resonance, whilst varying the photon energy of the excitation laser. In this measurement, the excitation laser is focused on the TMD area and the frequency is measured using a phase-locked-loop (PLL) (details in supplementary

information). In figure 2(a), we plot the frequency shift Δf (blue, left y-axis) and the corresponding incoming laser power P_{inc} (grey, right y-axis) vs. the photon energy of the excitation laser. Upon dividing the frequency shift by the laser power and normalizing it by f_0, we obtain the relative responsivity $R(E_\gamma) = \frac{\Delta f(E_\gamma)}{f_0 P_{\text{inc}}(E_\gamma)}$ (figure 2(b)). This signal is directly proportional to the absorption coefficient of the 2D material. Finally, we use the beforehand determined $R_{100\%}$ to calculate the absorption coefficient of the TDM in absolute units: $Abs(E_\gamma) = R(E_\gamma)/R_{100\%}$ — as plotted in figure 2(b) on the right y-axis. In this spectrum, we find clear peaks (A–D), that correspond
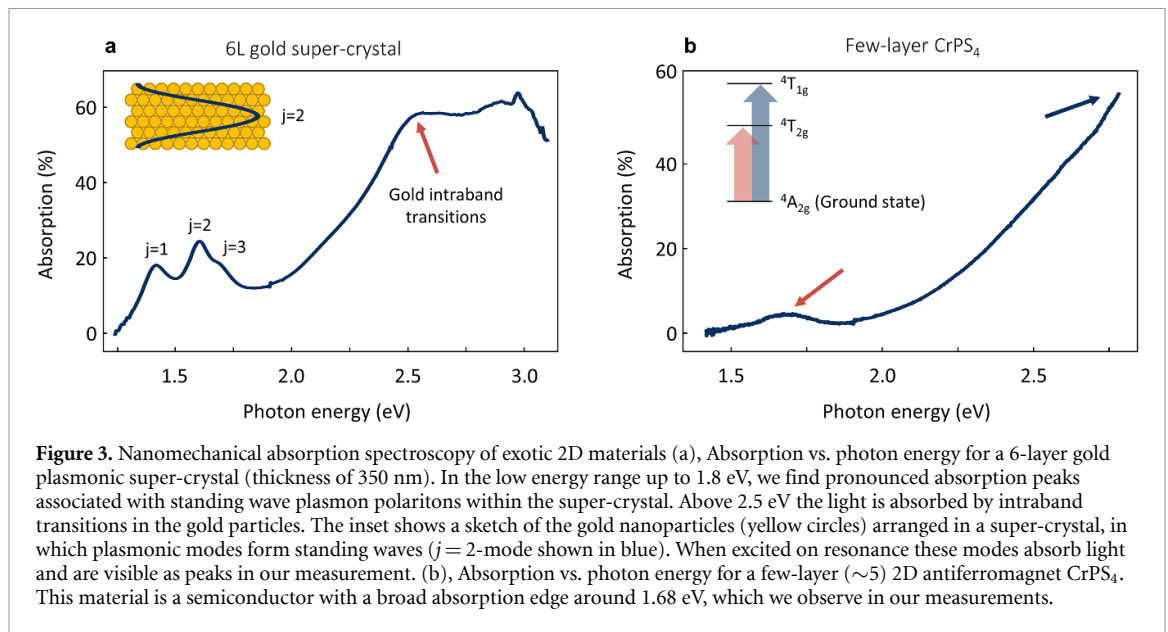
Figure 3. Nanomechanical absorption spectroscopy of exotic 2D materials (a), Absorption vs. photon energy for a 6-layer gold plasmonic super-crystal (thickness of 350 nm). In the low energy range up to 1.8 eV, we find pronounced absorption peaks associated with standing wave plasmon polaritons within the super-crystal. Above 2.5 eV the light is absorbed by intraband transitions in the gold particles. The inset shows a sketch of the gold nanoparticles (yellow circles) arranged in a super-crystal, in which plasmonic modes form standing waves ($j = 2$-mode shown in blue). When excited on resonance these modes absorb light and are visible as peaks in our measurement. (b), Absorption vs. photon energy for a few-layer ($\sim$5) 2D antiferromagnet CrPS$_4$. This material is a semiconductor with a broad absorption edge around 1.68 eV, which we observe in our measurements.

to different excitonic species at the expected energies [31]. In the inset, we sketch the corresponding transitions for few-layer WS$_2$ (following [31]). Some fraction of light will reach the SiN below the TMD and be absorbed there, which may lead to large relative measurement errors in the spectral range, where the TMD exhibits low absorption. To account for this, we perform the following correction: $\text{Abs}_{\text{2DM}} = \frac{\text{Abs}_{\text{total}} - \text{Abs}_{\text{SiN}}}{1 - \text{Abs}_{\text{SiN}}}$. This correction may introduce a small error in the region, where the 2D material exhibits large absorption as we potentially underestimate the absorption in SiN (details in supplementary information), but significantly reduces the relative error in the region of low absorption. SiN is an amorphous insulator with very weak light–matter interaction, resulting in low absorption ($\sim$0.5%) and a rather flat spectrum in the spectral region of interest, which justifies this step.

2.3. Characterizing exotic 2D materials

Next, we extend our method to study more exotic 2D materials. We choose two materials that are particularly suited for our method and for which it is expected to produce advantages. The first one is a layered crystal (super-crystal) made from plasmonic nanoparticles. These gold nanoparticles (diameter 56 nm) are embedded into a polymer matrix forming a closely spaced fcc super-crystal [19, 20]. Such super-crystals have been recently shown to enter the deep strong light–matter coupling regime, in which light within a material can no longer be seen as a perturbation to the properties of the material [19, 20]. Instead, the material properties are almost entirely determined by light–matter interaction [19, 20]. We grow the super-crystals by self-assembly on a liquid-liquid interface (details inf [19, 20, 32]), carefully transfer them

onto the SiN membranes by the PDMS dry transfer technique [30] and perform our nanomechanical absorption spectroscopy measurements. We note that for the highest accuracy, all samples are calibrated individually following the protocol described above for the WS$_2$ sample. In figure 3(a) we show the absorption spectrum obtained for a 6-layer super-crystal. Starting from low photon energies, we find three peaks associated with plasmonic modes within the super-crystal ($j = 1..3$ comp. inset figure 3(a)). As we go to higher energies, the absorption increases towards the intraband transitions of gold and plateaus around 2.5 eV. Interestingly, NMS works excellently despite the super-crystal being much thicker (350 nm vs. 2 nm) and also much heavier than the TMD studied above. Whilst the fundamental resonance frequency and the absolute shifts in frequency for this heavier sample are smaller, the quality factor, responsivity and thus the sensitivity remain comparable to the lighter samples. Plasmonic structures are known to scatter a significant amount of light that cannot be distinguished from absorbed light by common optical measurement methods. In contrast, NMS is only sensitive to absorbed light and therefore ideal to study plasmonic systems.

Our second choice is a 2D antiferromagnet CrPS$_4$ with a Néel temperature for the bulk material of $T_{\text{Neel}} = 36$ K [33]. The study of 2D magnetism requires measurements at low temperatures and high magnetic fields, which is challenging for conventional optics but is easier using NMS. We exfoliate and transfer a few-layer (approx. 5) thick flake of CrPS$_4$ onto a SiN membrane and perform NMS (see figure 3(b)). In the spectrum, we find a broad peak around 1.68 eV. This peak belongs to the $d-d$ transition of the Cr^{3+} ions from the $^4A_{2g}$ to the $^4T_{2g}$ state. Towards higher photon energies the absorption
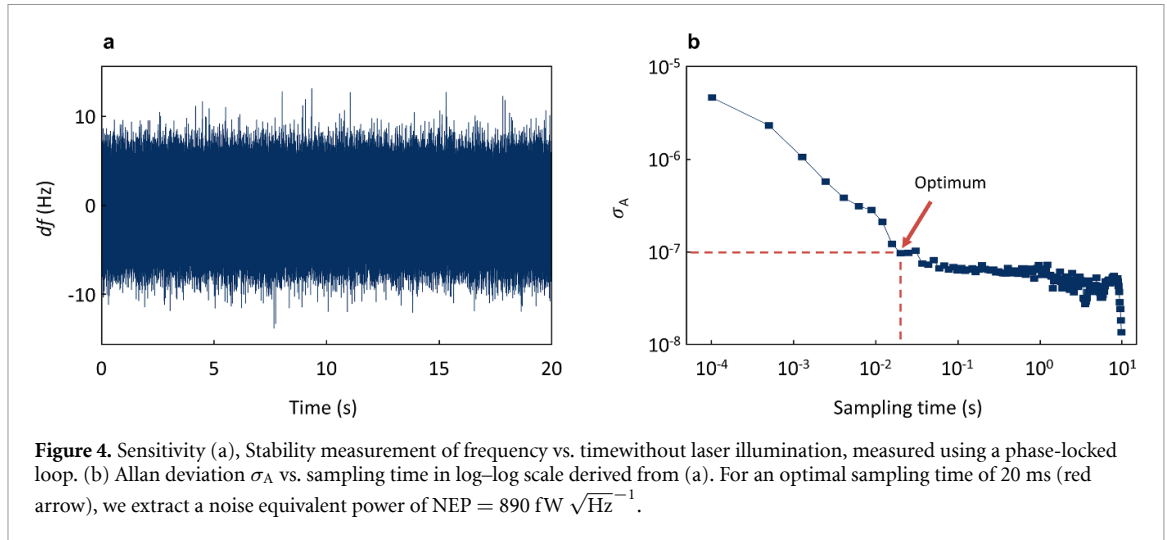
Figure 4. Sensitivity (a), Stability measurement of frequency vs. timewithout laser illumination, measured using a phase-locked loop. (b) Allan deviation σ_A vs. sampling time in log–log scale derived from (a). For an optimal sampling time of 20 ms (red arrow), we extract a noise equivalent power of NEP = 890 fW $\sqrt{\mathrm{Hz}}^{-1}$.

increases, as we approach higher-order transitions (e.g. $^4\mathrm{A}_{2g}$ to $^4\mathrm{T}_{1g}$). This spectrum measured above the antiferromagnet's Néel temperature is expected and in line with literature reports [33–35]. Thin $CrPS_4$ is rather sensitive to photodamage [33, 35], which can be problematic for classical optical approaches. For NMS however small laser powers ($P_{inc} \approx 1\ \mu$W) are sufficient to induce sizeable frequency shifts (comp. figure 2(a)), which can help preserve the quality of sensitive samples. At the same time, the heating-related temperature changes of our samples (see supplementary information) are small, and we can assume that the thermal constants are unaffected by the laser beam. Overall, we have spectroscopically characterized a range of exotic 2D materials with high resolution and believe that these measurements highlight the broad applicability of NMS.

2.4. Sensitivity

In order to compare NMS to state-of-the-art optical approaches, we determine its sensitivity (noise equivalent power *NEP*) and response time (τ). In our measurements, we use frequency shifts to probe the amount of absorbed light. In order to quantify the noise in our measurements, we, therefore, look at frequency fluctuations, which we then convert into power noise using $R_{100\%}$ [10, 18, 36–38]. Assuming white noise, the *NEP* can be derived from the fractional frequency noise power spectral density ($S_y(0)$) and is given by [39, 40]:

$$\mathrm{NEP} = \frac{\sqrt{S_y(0)}}{R_{100\%}} = \frac{\sigma_A \sqrt{2 t_{sampling}}}{R_{100\%}} \qquad (1)$$

where σ_A is the Allan deviation of the frequency measurement [41] and $t_{sampling}$ is the sampling time. To obtain σ_A, we perform a frequency stability measurement in the PLL configuration with the excitation laser turned off (figure 4(a)). From this data, we derive σ_A vs. sampling time (figure 4(b)). We choose an optimal value of $\sigma_A = 9.7 \times 10^{-8}$ for $t_{sampling} =$

20 ms and using $R_{100\%} = 21\,810$ W^{-1}, we obtain NEP = 890 fW $\sqrt{\mathrm{Hz}}^{-1}$. This value is two orders of magnitude lower than in our previous approach (NEP = 90 pW $\sqrt{\mathrm{Hz}}^{-1}$) [18].

The sensitivity of NMS is now comparable to commercially available avalanche photodetectors (APDs) for the same spectral range with NEP = 200 fW $\sqrt{\mathrm{Hz}}^{-1}$ (Thorlabs APD130A(/M)). APDs are highly sensitive, but also overload quickly. Compared to these commercial devices, NMS-based devices show a higher dynamic range (84 dB vs. 69 dB—both for 1 s integration time) and can easily detect hundreds of μW (details in supplementary information).

To assess the measurement speed of NMS, we simulate time-dependent laser heating in our sample and extract a response time for our mechanical system of $\tau = 800\ \mu$s (simulations in supplementary information), which is in line with experimental data on similar devices [37, 39]. The fast response time, allows us to sweep the excitation energy rapidly and we obtain the Δf vs. E_γ traces presented above in a matter of seconds.

3. Discussion

We presented a simplified and improved method of nanomechanical absorption spectroscopy. With a sensitivity of NEP = 890 fW $\sqrt{\mathrm{Hz}}^{-1}$ and a response time $\tau = 800\ \mu$s, the method now is a promising alternative to classical optical approaches, whilst it overcomes long-standing limitations. At the same time, we show that using SiN as a reference material provides a robust and straightforward calibration. We demonstrated the broad applicability of NMS by spectroscopically characterizing a 2D semiconductor, a layered plasmonic super-crystal and a novel 2D antiferromagnet. The key points for the improvement of the measurement sensitivity are stress reduction in the SiN membranes and thermal decoupling of

the 2D material, which leads to enhanced responsivity and improved sensitivity. The responsivity almost entirely depends on the thermal properties of the SiN membrane. Therefore, we expect a sensitivity mostly independent of the thermal properties of the 2D materials (details in supplementary information). To further reduce *NEP*, we could use temperature regulation of the sample to controllably minimize the tensile stress σ_0. Upon cooling the sample, the silicon frame shrinks more than the suspended SiN membrane, due to their difference in thermal expansion coefficient. This reduces the stress in the suspended SiN and would allow measuring very close to $\sigma_0 = 0$, which would mean further increased responsivity and thus improved sensitivity. We note that in comparison to our previous experiments, the 2D material is not suspended in this work but in direct contact with the SiN. This changes the dielectric environment of the 2D material and can affect excitons and other quasiparticles in 2D materials. We find that this has a large impact on photoluminescence measurements, where it completely suppresses the emission (see supplementary information), but does not affect absorption spectra [42]. The suppressed emission suggests a very low quantum yield ($<10^{-6}$), which justifies the assumption that all the absorbed light is converted into heat and therefore detected by NMS.

We also aim to characterize 2D materials at low temperatures using NMS. In the limit of $T \to 0$ K, the specific heat of any material goes to zero and along with it the thermal conductivity κ and thermal expansion coefficient α. If α decreases faster than κ, our method will not work anymore, because the responsivity is proportional to $\frac{\alpha}{\kappa}$ [23]. To exclude this scenario, we do preliminary measurements of the responsivity of a bare SiN membrane as a function of temperature. For this, we use a membrane with higher pre-stress ($\sigma_0 = 240$ MPa) to avoid buckling upon cooldown and find that even at 4.2 K, the membrane shows considerable responsivity (see supplementary information). This paves the way for future experiments at low temperatures and will allow the unlocking of exciting physics in a large range of 2D materials.

Data availability statement

All data that support the findings of this study are included within the article (and any supplementary files).

Acknowledgments

ORCID iDs

Jan N Kirchhof ● https://orcid.org/0000-0001-8576-4787
Denis Yagodkin ● https://orcid.org/0000-0002-9135-8918
Daniel B de Araújo ● https://orcid.org/0000-0001-5216-6035
Samuel Manas-Valero ● https://orcid.org/0000-0001-6319-9238
Eugenio Coronado ● https://orcid.org/0000-0002-1848-8791
Herre van der Zant ● https://orcid.org/0000-0002-5385-0282
Stephanie Reich ● https://orcid.org/0000-0002-2391-0256
Silvan Schmid ● https://orcid.org/0000-0003-3778-7137
Kirill I Bolotin ● https://orcid.org/0000-0003-1821-3429

References

[1] De Bonis S, Urgell C, Yang W, Samanta C, Noury A, Vergara-Cruz J, Dong Q, Jin Y and Bachtold A 2018 *Nano Lett.* **18** 5324–8
[2] Weber P, Güttinger J, Noury A, Vergara-Cruz J and Bachtold A 2016 *Nat. Commun.* **7** 1–8
[3] Eichler A 2022 *Mater. Quantum Technol.* **2** 043001
[4] Chaste J, Eichler A, Moser J, Ceballos G, Rurali R and Bachtold A 2012 *Nat. Nanotechnol.* **7** 301–4
[5] Chiu H Y, Hung P, Postma H W C and Bockrath M 2008 *Nano Lett.* **8** 4342–6
[6] Lemme M C *et al* 2020 *Research* **2020** 8748602
[7] Desai S H, Pandya A A and Panchal M B 2021 *J. Phys.: Conf. Ser.* **1854** 012029
[8] Lee H L, Yang Y C and Chang W J 2013 *Jpn. J. Appl. Phys.* **52** 025101
[9] Steeneken P G, Dolleman R J, Davidovikj D, Alijani F and Van der Zant H S 2021 *2D Mater.* **8** 042001
[10] Blaikie A, Miller D and Alemán B J 2019 *Nat. Commun.* **10** 1–8
[11] Wittmann S, Glacer C, Wagner S, Pindl S and Lemme M C 2019 *ACS Appl. Nano Mater.* **2** 5079–85
[12] Jiang S, Xie H, Shan J and Mak K F 2020 *Nat. Mater.* **19** 1295–9
[13] Verbiest G J, Kirchhof J N, Sonntag J, Goldsche M, Khodkov T and Stampfer C 2018 *Nano Lett.* **18** 5132–7
[14] Baglioni G, Pezone R, Vollebregt S, Cvetanovic K, Spasenovic M, Todorovic D, Liu H, Verbiest G J, van der Zant H S J and Steeneken P G 2022 Ultra-sensitive graphene membranes for microphone applications (arXiv:2211.03369)
[15] Pezone R, Baglioni G, Sarro P M, Steeneken P G and Vollebregt S 2022 *ACS Appl. Mater. Interfaces* **14** 21705–12
[16] Dolleman R J, Chakraborty D, Ladiges D R, van der Zant H S J, Sader J E and Steeneken P G 2021 *Nano Lett.* **21** 7617–24
[17] Rosłoń I E, Japaridze A, Steeneken P G, Dekker C and Alijani F 2022 *Nat. Nanotechnol.* **17** 637–42

[18] Kirchhof J N, Yu Y, Antheaume G, Gordeev G, Yagodkin D, Elliott P, de Araújo D B, Sharma S, Reich S and Bolotin K I 2022 *Nano Lett.* **22** 8037–44

[19] Mueller N S, Okamura Y, Vieira B G, Juergensen S, Lange H, Barros E B, Schulz F and Reich S 2020 *Nature* **583** 780–4

[20] Mueller N S, Pfitzner E, Okamura Y, Gordeev G, Kusch P, Lange H, Heberle J, Schulz F and Reich S 2021 *ACS Nano* **15** 5523–33

[21] Schmid S *et al* 2014 *J. Appl. Phys.* **115** 054513

[22] Schwarz C, Pigeau B, Mercier de Lépinay L, Kuhn A G, Kalita D, Bendiab N, Marty L, Bouchiat V and Arcizet O 2016 *Phys. Rev. Appl.* **6** 064021

[23] Chien M H, Brameshuber M, Rossboth B K, Schütz G J and Schmid S 2018 *Proc. Natl Acad. Sci.* **115** 11150–5

[24] Verbridge S S, Parpia J M, Reichenbach R B, Bellan L M and Craighead H G 2006 *J. Appl. Phys.* **99** 124304

[25] Schmid S, Jensen K D, Nielsen K H and Boisen A 2011 *Phys. Rev.* B **84** 165307

[26] Luke K, Dutt A, Poitras C B and Lipson M 2013 *Opt. Express* **21** 22829–33

[27] Fong K Y, Pernice W H P and Tang H X 2012 *Phys. Rev.* B **85** 161410

[28] Ftouni H, Blanc C, Tainoff D, Fefferman A D, Defoort M, Lulla K J, Richard J, Collin E and Bourgeois O 2015 *Phys. Rev.* B **92** 125439

[29] Luhmann N, Jachimowicz A, Schalko J, Sadeghi P, Sauer M, Foelske-Schmitz A and Schmid S 2017 *Appl. Phys. Lett.* **111** 063103

[30] Castellanos-Gomez A, Buscema M, Molenaar R, Singh V, Janssen L, van der Zant H S J and Steele G A 2014 *2D Mater.* **1** 011002

[31] Goswami T, Bhatt H, Babu K J, Kaur G, Ghorai N and Ghosh H N 2021 *J. Phys. Chem. Lett.* **12** 6526–34

[32] Bastús N G, Comenge J and Puntes V 2011 *Langmuir* **27** 11098–105

[33] Lee J, Ko T Y, Kim J H, Bark H, Kang B, Jung S G, Park T, Lee Z, Ryu S and Lee C 2017 *ACS Nano* **11** 10935–44

[34] Gu P *et al* 2020 *ACS Nano* **14** 1003–10

[35] Kim S, Yoon S, Ahn H, Jin G, Kim H, Jo M H, Lee C, Kim J and Ryu S 2022 *ACS Nano* **16** 16385–93

[36] Kurek M, Carnoy M, Larsen P E, Nielsen L H, Hansen O, Rades T, Schmid S and Boisen A 2017 *Angew. Chem., Int. Ed.* **56** 3901–5

[37] Piller M, Hiesberger J, Wistrela E, Martini P, Luhmann N and Schmid S 2023 *IEEE Sens. J.* **23** 1066–71

[38] Piller M, Luhmann N, Chien M H and Schmid S 2019 Nanoelectromechanical infrared detector *Proc. SPIE* **11088** 9–15

[39] Snell N, Zhang C, Mu G, Bouchard A and St-Gelais R 2022 *Phys. Rev. Appl.* **17** 044019

[40] Vig J and Kim Y 1999 *IEEE Trans. Ultrason. Ferroelectr. Freq. Control* **46** 1558–65

[41] Allan D W 1966 *Proc. IEEE* **54** 221–30

[42] Li Y, Chernikov A, Zhang X, Rigosi A, Hill H M, van der Zande A M, Chenet D A, Shih E M, Hone J and Heinz T F 2014 *Phys. Rev.* B **90** 205422